Geophysical Research Letters

RESEARCH LETTER
10.1029/2020GL088119

Key Points:
- Three 4-year-long mooring time series show anomalously warm and prolonged inflow along the eastern flank of the Filchner Trough in 2017
- Warm water persists on the shelf throughout winter and is associated with a fresh anomaly that leads to changes in the shelf density structure
- We hypothesize that the fresh anomaly originated from anomalous summer sea ice melt upstream and caused shoaling of shelf break thermocline

Supporting Information:
- Supporting information S1
- Figure S1
- Figure S2
- Figure S3

Correspondence to:
S. Ryan,
sryan@whoi.edu

Citation:
Ryan, S., Hellmer, H. H., Janout, M., Darelius, E., Vignes, L., & Schröder, M. (2020). Exceptionally warm and prolonged flow of Warm Deep Water toward the Filchner-Ronne Ice Shelf in 2017. *Geophysical Research Letters*, *47*, e2020GL088119. https://doi.org/10.1029/2020GL088119

Received 24 MAR 2020
Accepted 3 JUN 2020
Accepted article online 9 JUN 2020

Exceptionally Warm and Prolonged Flow of Warm Deep Water Toward the Filchner-Ronne Ice Shelf in 2017

Svenja Ryan[1,2], Hartmut H. Hellmer[1], Markus Janout[1], Elin Darelius[3], Lucie Vignes[4], and Michael Schröder[1]

[1]Alfred Wegener Institute, Helmholtz Centre for Polar and Marine Research, Bremerhaven, Germany, [2]Now at Woods Hole Oceanographic Institution, Woods Hole, MA, USA, [3]Geophysical Institute, University of Bergen, Bergen, Norway, [4]Laboratoire d'Océanographie et du Climat, Sorbonne Université/CNRS, Paris, France

Abstract The Filchner-Ronne Ice Shelf, fringing the southern Weddell Sea, is Antarctica's second largest ice shelf. At present, basal melt rates are low due to active dense water formation; however, model projections suggest a drastic increase in the future due to enhanced inflow of open-ocean warm water. Mooring observations from 2014 to 2016 along the eastern flank of the Filchner Trough (76°S) revealed a distinct seasonal cycle with inflow if Warm Deep Water during summer and autumn. Here we present extended time series showing an exceptionally warm and long inflow in 2017, with maximum temperatures exceeding 0.5°C. Warm temperatures persisted throughout winter, associated with a fresh anomaly, which lead to a change in stratification over the shelf, favoring an earlier inflow in the following summer. We suggest that the fresh anomaly developed upstream after anomalous summer sea ice melting and contributed to a shoaling of the shelf break thermocline.

1. Introduction

The ice shelves fringing the Antarctic continent are central to the stability of the Antarctic Ice Sheet, whose mass balance is largely controlled by the interaction of the ice shelves with the ocean (Fürst et al., 2016). Enhanced basal melt rates and ice shelf thinning have been observed widely during the last decade, in particular in the Bellingshausen and Amundsen Seas (e.g., Paolo et al., 2015; Rignot et al., 2013). These changes have mostly been attributed to an increased transport of warm middepth Circumpolar Deep Water (CDW) onto the continental shelf (Nakayama et al., 2013; Pritchard et al., 2012). The exchange of water masses across the continental shelf break is largely controlled by dynamics and characteristics of the near-circumpolar Antarctic Slope Front (ASF; Jacobs, 1991) and the associated Antarctic Slope Current (ASC; see Thompson et al., 2018, for a review). The ASF and cross-slope exchange respond to local wind forcing (Gill, 1973; Graham et al., 2013; Stewart & Thompson, 2015)-mainly the along-coast component of the Antarctic easterlies-but also to buoyancy forcing, which is dominated by the seasonal sea ice cycle next to local input of glacial melt water (Hattermann, 2018; Núñez-Riboni & Fahrbach, 2009; Nøst et al., 2011). Furthermore, earlier studies suggest that complex processes such as dense water overflows, tides, and baroclinic instabilities can significantly influence the cross-slope and cross-shelf transport (Nøst et al., 2011; Stewart & Thompson, 2015; Stewart et al., 2018; St-Laurent et al., 2013).

The southeastern Weddell Sea, home of the large Filchner-Ronne Ice Shelf (FRIS), is of great climatic importance as dense water production on the 400 km broad continental shelf contributes significantly to the formation of Weddell Sea Deep and Bottom Waters (Nicholls et al., 2009). Both water masses are precursors of the globally relevant Antarctic Bottom Water (Foldvik, 2004), which ventilates the abyssal ocean (Reid & Lynn, 1971) and supplies the lower limb of the global overturning circulation (Sloyan & Rintoul, 2001). The Filchner Trough (FT, Figure 1) connects the deep ocean with the FRIS cavity, serving as outflow pathway of the potentially supercooled Ice Shelf Water (ISW; Darelius et al., 2014; Foldvik & Gammelsrød, 1988). ISW is formed by the interaction of High Salinity Shelf Water with the ice shelf base, resulting in temperatures below the surface freezing point (θ<−1.9°C). The trough also provides a potential inflow pathway for Modified Warm Deep Water (MWDW), a product of mixing at the ASF where open-ocean, middepth Warm Deep Water (WDW)-a derivative of CDW-mixes with the overlying Winter Water (WW). Seasonal intrusions of MWDW are observed at depth (~200–400 m) along FT's eastern flank and over the shallower eastern shelf (depth ~<450 m) during summer and autumn (approximately January–May; Årthun et al., 2012; Ryan et al.,

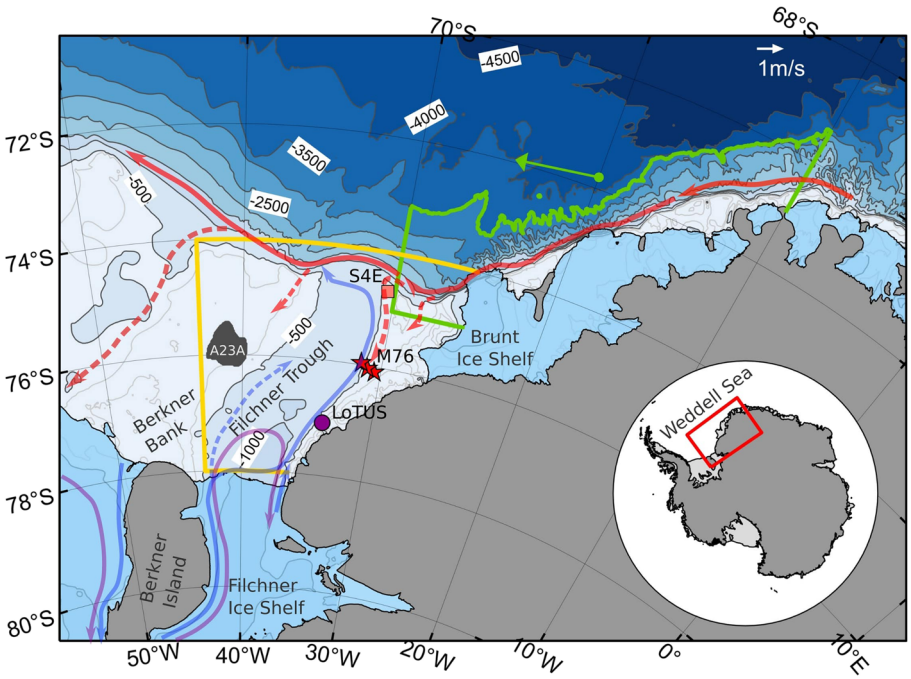

Figure 1. Bathymetric map of the study region and schematic ocean circulation after Darelius et al. (2014), Darelius and Sallée (2018), and Nicholls et al. (2009). Arrows represent the flow of Warm Deep Water (solid red), intrusions of Modified Warm Deep Water (dashed red), and Ice Shelf Water (blue and purple), with dashed blue indicating potential pathways. The positions of moorings (M76) and LoTUS buoy are labeled. Wind stress (ERA-Interim) and sea ice concentration (SSMI) are averaged within the green (Box_{ups}) and yellow (Box_{loc}) boxes with each box bounded by the coast. Ice shelves are marked in light blue and grounded ice/land in gray. Bathymetry is shown in blue shading with contours every 500 m (dark gray) and every 100 m in regions shallower than 1,000 m (light gray). The green arrow shows direction and strength of the mean (2002–2018) wind stress in Box_{ups}. The inset shows the location of the study region.

2017). The seasonality has been linked to weaker along-coast wind stress during summer (all seasons are austral seasons), driving a shoaling of the ASF. Mooring data from the eastern shelf from 2013–2016 show a cessation of the warm inflow around June, followed by temperatures persisting around the surface freezing point or below throughout winter and spring (Ryan et al., 2017). In 2013, MWDW was observed in the vicinity of the Filchner Ice Shelf (FIS) front at the end of summer, as a results of a strengthened wind-driven coastal current (Darelius et al., 2016). While basal melt rates have been stable under FRIS to date (Paolo et al., 2015; Rignot et al., 2019), numerical model simulations predict that in a future warming climate MWDW may irreversibly enter the continental shelf via the FT and ultimately fill the FRIS cavity causing enhanced basal melting (Hellmer et al., 2012; Timmermann & Hellmer, 2013). FRIS is by volume the largest Antarctic ice shelf and buttresses several ice streams draining the Antarctic Ice Sheet (east and west) and therefore can potentially contribute several meters to sea level rise. Additionally, increased freshwater input from enhanced melting would ultimately affect the local dense water formation as shelf waters would become more buoyant leading to a shutdown of Ice Shelf Water formation and a flushing of the ice shelf cavity with MWDW (Hellmer et al., 2017). Thus, continuous efforts are being undertaken to monitor the warm inflow and understand key processes in the region.

This paper presents three extended mooring time series from the eastern flank of the FT that were installed from 2014 to 2018. The data reveal a particularly warm and prolonged inflow in 2017, compared to previous years. Hydrographic properties and possible forcing mechanisms of this event are investigated in this study.

2. Data

Three moorings were operated on the southeastern Weddell Sea continental shelf (Figure 1) between 2014 and 2018. They were oriented zonally along 76°S at depths between 450 m ($M_{30.5W}$ at 30.47°W, 76.09°S; M_{31W} at 30.99°W, 76.05°S) and 580 m ($M_{31.5W}$ at 31.48°W, 75.96°S). Temperature, salinity, and pressure were recorded at two depth levels (330 m and at bottom), with additional temperature measurements from 2016 to

2018. (For details on mooring deployment see supporting information Table S1 and Janout et al., 2019; Schröder & Wisotzki, 2014; Schröder et al., 2016).

Conductivity-temperature-depth (CTD) profiles were collected during deployment and recovery cruises as well as during the ES060 (RRS *Earnest Shackleton* Darelius & Fer, 2015) and WAPITI (JR16004, RSS *James Clark Ross* Sallée, 2018) expeditions in 2013 and 2017, respectively. A Long Term Underwater System (LoTUS) buoy was deployed at 77.09°S, 33.77°W (~384 m depth) during 2017 (see Table S1 for details Darelius & Kuttenkueler, 2018).

Wind velocity at 10 m above sea level was obtained from the ERA-Interim reanalysis product with a horizontal resolution of 0.75° (Dee et al., 2011) and used to derive the surface wind stress following the method by Andreas et al. (2010), which implements changes to the drag coefficient depending on the sea ice concentration (see supporting information for more details on calculation). For consistency in the horizontal grid ERA sea ice concentrations are used for the calculation. For Box_{ups} (green in Figure 1), the coordinate system is rotated to 245° to obtain the along-coast component. An extended time series (2002–2017) of polynya ice production rates derived for winter (April–September) is used (Paul et al., 2015b), which were computed from daily Moderate-Resolution Imaging Spectroradiometer (MODIS) median thin-ice thickness composites. Daily SSMI-SSMIS sea ice concentration data were obtained as a 5-day median-filtered and gap-filled product from the Integrated Climate Data Center in Hamburg (ICDC), Germany.

3. Results

3.1. Prolonged and Exceptionally Warm Inflow in 2017

The hydrography along the eastern flank of the FT typically shows a distinct seasonal cycle with MWDW inflow during summer/autumn ($-1.5 \leq \theta \leq -1$°C), followed by a decrease to near-freezing temperatures in winter, driven by a combination of seasonal suppression of the shelf break thermocline and local surface freezing and the development of deep mixed layers (Ryan et al., 2017; Figure 2). The seasonality is generally a robust feature in the 4-year record from 2013–2016. In 2017, an unprecedented strong and long warm inflow was observed across the whole mooring array (Figures 2a–2c) with maximum temperatures exceeding those previously observed by up to ~0.5°C (i.e., $\sigma > -1$°C). The maximum temperatures are also associated with higher salinity (and density, Figures 2d–2f), which suggests the inflow to be composed of denser WDW, commonly found at greater depths over the continental slope. Alternatively, there has been less mixing with the overlaying WW during the cross-slope exchange.

In stark contrast to the previously observed seasonal cycle, temperatures at $M_{30.5W}$ and M_{31W} remain above freezing until October, around −1.7°C and −1.5°C at ~330 and ~430 m, respectively. Thus, warmest water is found along the bottom. Cold and saline spikes between July and October near the bottom at M_{31W} (Figures 2b and 2h) suggest lateral/vertical movement of the ISW/MWDW interface past the mooring. The absence of these spikes at $M_{30.5W}$ (Figures 2a and 2g) suggest that the interface remains to the east of it. Temperatures above freezing (~−1.7°C), are also found over the slope at $M_{31.5W}$ during winter (Figures 2c and 2i), however, the temperature is generally lower than at M_{31W} and $M_{30.5W}$, suggesting that the core of prolonged warm inflow is confined to the shallower eastern shelf. Observations at ~77°S-384 m (Figure 2c, yellow line) show maximum temperatures above −1.5°C in autumn, which is close to the temperatures observed at this latitude during the strong warm inflow observed in 2013 (see $\mathrm{M77}_{NORTH}$Darelius et al., 2016). In agreement with the observations at 76° S, temperatures remain above freezing between July and October. The LoTUS buoy was located at approximately 384 m depth; mooring observations in 2013 indicate that the main warm core follows the 400–500 m isobath and might therefore not have been fully captured by the LoTUS buoy. These results suggests that MWDW may have reached the FIS front in 2017, similarly to 2013 (Darelius et al., 2016).

3.2. Fresh Anomaly

After peak temperatures are reached in late autumn, decreasing temperatures are generally associated with a continuous freshening (Figures 2g–2i), due to increased entrainment of upper-layer WW as the shelf break thermocline deepens (Årthun et al., 2012). In 2014–2016, salinity on the eastern shelf ($M_{30.5W}$ and M_{31W}) reached a minimum in June/July (~34.4) in concert with the cessation of the warm inflow and followed by a gradual salinity increase during winter. In 2017, however, the increase in salinity is absent and

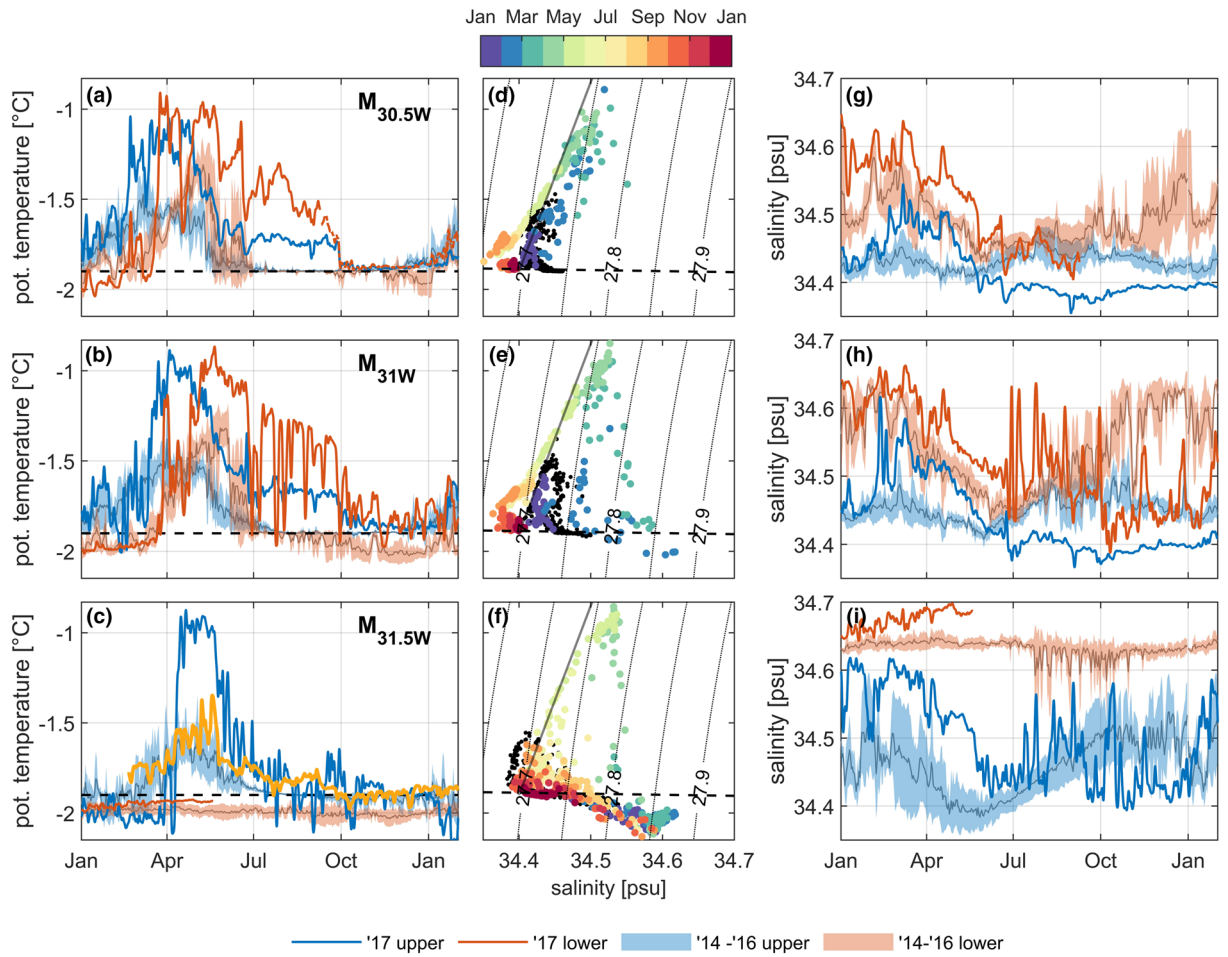

Figure 2. Low-pass filtered (3 days) potential temperature (a–c) and salinity (g–i) time series at all three moorings for 2017 and the mean seasonal cycle from 2014–2016 (shading) for the upper (blue) and bottom (red) instruments at $M_{30.5W}$ (330 and 430 m), M_{31W} (340 and 430 m), and $M_{31.5W}$ (330 m [380 m second deployment] and 565 m). (d–f) TS diagram of 2017 upper sensor data (daily mean values) with time in color and mean annual cycle (2014–2016) as black points. Yellow line in (c) is time series of LoTUS buoy in 2017, and the gray line in (d)–(f) is a reference for the MWDW mixing line. The bottom sensor at $M_{30.5W}$ stopped working in September; temperature from the thermistor above (415 m) is shown (dashed line in a) for the remainder of the year.

continuous freshening is observed instead over the eastern shelf. The salinity minimum is reached around October ($S \leq 34.4$) and coincides with the termination of the warm signal on the eastern shelf (31°W, 30.5°W). The freshest water is found at middepth (upper sensors) on the eastern shelf, particularly at $M_{30.5W}$, suggesting advection by the coastal current as a potential source of the freshening.

In Temperature-Salinity (TS) space, MWDW lays on the mixing line between WDW and WW (gray line in Figures 2d and 2e). The MWDW observed on the eastern shelf during winter in 2017 indicates mixing with a slightly fresher end-member than in previous years (Figures 2d and 2e). These properties resemble Eastern Shelf Water (ESW), which is generally found upstream of the FT on the narrow continental shelf, where Ekman-driven downwelling transports surface water, further freshened by input of glacial meltwater, to greater depth (Fahrbach et al., 1994). Thus ESW typically has lower salinities compared to WW, while both have temperatures close to the freezing point ($34.28 \leq S \leq 34.40$; Carmack, 1974).

In 2014–2016, the ISW layer (cold, saline) extended onto the eastern shelf along the bottom from about October onward, with ISW being observed at M_{31W} almost continuously every autumn, while reaching as far as $M_{30.5W}$ sporadically (Ryan et al., 2017; Figures 2a, 2b, 2g, and 2h). This is not observed in 2017. The combination of the freshening signal and the absence of salinification during winter, leads to significantly fresher conditions on the eastern shelf at the beginning of the following summer (December 2017) compared to previous years at this time.

Hence, 2017 was not just characterized by a warmer and prolonged warm inflow but also a pronounced fresh anomaly. In the next section, the resulting changes in the vertical density structure and implications are investigated further.

4. Modified Shelf Density Structure

A Hovmoeller diagram of temperature at $M_{31.5W}$ from 2016 to 2018 (Figure 3a) shows that generally the upper interface of ISW (−1.9°C isotherm), lays above 380 m during summer and deepens in the presence of the warm intrusions, extending down to a depth of approximately 500 m in late autumn. In 2016, temperatures between ∼380- to 500-m depth decrease in late autumn and reach the surface freezing point in August, indicated by a sharp jump and subsequent vanishing of the −1.9°C isotherm. At the same time, ISW appears in the bottom layer at M_{31W} (not shown) in agreement with the seasonal cycle described by Ryan et al. (2017).

In 2017, significantly warmer temperatures (> -1.2°C) are present (Figure 3a) and extend down to 500 m in May/June. In contrast to 2016 (and likely to previous years), the ISW interface shoals only gradually while warmer water remains present at middepth throughout winter. In January 2018, the ISW layer ultimately extends to above the upper sensor, that is, ∼380 m. CTD profiles in the FT (depth > 500 m) from February 2018 show that the upper 400 m of the water column remain about 0.1 kg m^{-3} lighter (∼0.5–1 psu fresher) compared to 2013 and 2016 (Figure 3b). This indicates that the observed fresh water anomaly during winter 2017 altered the density structure over the FT significantly. This is also visible in the comparison of CTD sections along 76°S from different years (2013, 2014, 2016, 2018; see Figure S1).

MWDW entering the continental shelf in summer typically covers a density range between 27.7 and 27.8 kg m^{-3} (Figures 2d–2f). The bottom layer over the eastern shelf and at middepth (∼400 m) in the FT (at 76°S) had densities above 28.0 kg m^{-3} in summers (January/February) of 2013, 2014, and 2016 (Figures 3c and S1), thus "blocking" the lighter MWDW at these depth levels. In 2018 however, the hydrographic section at 76°S suggests that the modified density structure in the upper 400 m allows for an earlier warm water inflow at greater depth, in particular over the FT (Figure S1) but also over the eastern shelf where in previous years MWDW did not appear at the lower sensor of M_{31W} until the second half of March (Figure 2 Ryan et al., 2017). This could potentially lead to larger southward heat transport in 2018, however no data extending beyond February 2018 is available yet.

5. Wind and Sea Ice as Dominant Drivers

5.1. Shoaled Thermocline

CTD profiles at the shelf break east of the FT (Figures 4a and 4b) show that in 2014 the thermocline is suppressed below the shelf break depth (∼600 m) close to the Brunt Ice Shelf (yellow), while in 2017, profiles at similar positions, suggest a shallower thermocline (Δ∼50–100 m, orange). Profiles in both years were obtained in the first half of February (8–10 February). In addition, warm temperatures of up to −0.5°C are observed along the bottom further south within a small trough cutting across the continental shelf between the FT and Brunt Ice Shelf (blue). In contrast, nearby profiles from 2014 (purple) show temperatures below −1.5°C, suggesting weaker or no warm inflow via this trough. CTD casts only provide snapshots in time, however, the combination of the shallower thermocline and the presence of warmer water on the shelf further south, indicate that a stronger heat flux onto the continental shelf is already occurring east of the FT in 2017, due to a shoaled thermocline.

To investigate upstream versus local wind forcing, we define two near-shore boxes (see Figure 1). The along-slope wind stress at the end of 2016/beginning of 2017 in both boxes does not show a strong negative anomaly, which would support a relaxation of the ASF, compared to climatological values (Figure 4c). There is even a general tendency to above-average easterly wind stress between November and February, thus, neither local nor remote wind forcing is favoring a shoaling of the thermocline during summer (Figure 4c). Below-average wind stress is found in both boxes during March and April, potentially leading to a relaxation of the thermocline. A 3-year time series from a shelf break mooring located at the mouth of the FT between 2007 and 2009 (S4E, Figure 1; Årthun et al., 2012) indicates that the thermocline generally reaches its shallowest position toward the end of March. Afterward it deepens rather rapidly within 1 month

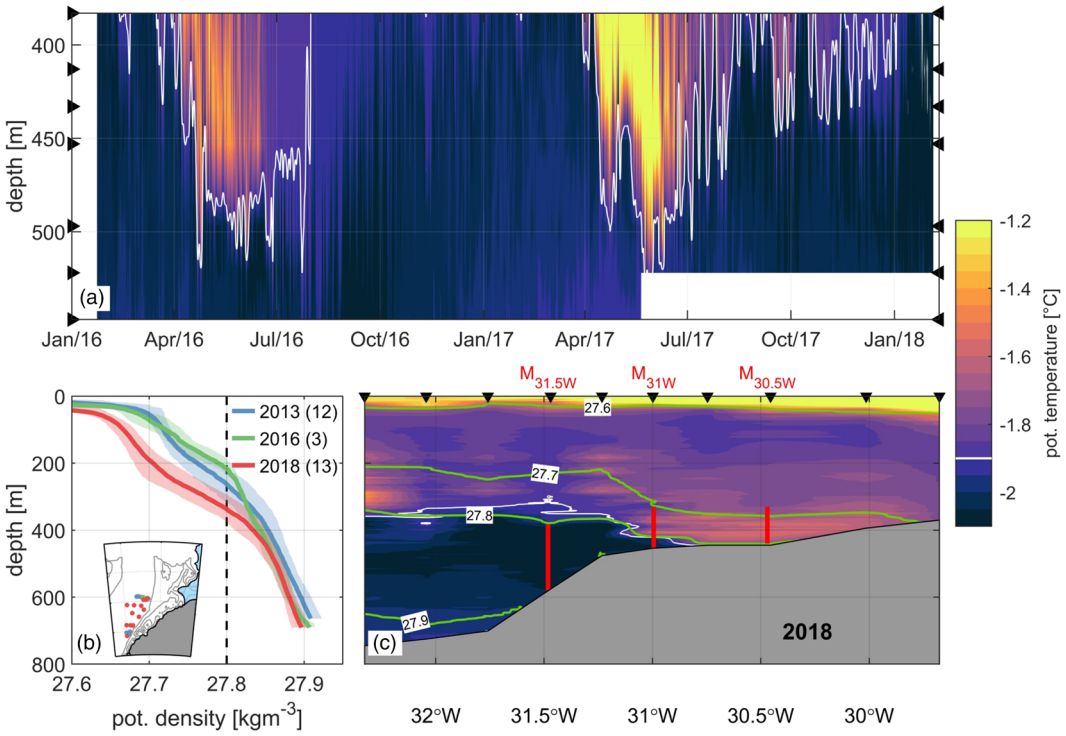

Figure 3. (a) Hovmoeller diagram of potential temperature at $M_{31.5W}$ (2016–2017). The white contour marks the −1.9°C isotherm, and black triangles mark the depth of sensors. (b) Means and associated standard deviation (shading) of selected density summer profiles from 2013, 2016, and 2018 from the Filchner Trough. (c) Hydrographic temperature section along 76°S in February 2018. The positions of the moorings (red lines), isopycnals (green contour lines), and the −1.9°C isotherm (white line) are shown. Black triangles mark stations used for the plotting the section.

below the shelf break depth of around 450 m (Ryan et al., 2017), "shutting off" the WDW supply. Interannual variability at S4E shows that weak wind stress in autumn (April–June) 2007 is associated with a longer and shallower presence of WDW at the shelf break (Årthun et al., 2012; Figure S3). Thus, the autumn wind stress anomalies in 2017 potentially contributed to a shallower thermocline depth and a prolonged inflow, however, this remains speculative as no shelf break observation are available yet during this time. While the along-coast wind forcing in autumn 2017 was favorable for a prolonged onshore flow and southward transport of MWDW, the high temperature of the inflow and the suggested thermocline shoaling upstream of the FT cannot be explained by the wind stress.

5.2. Thermocline Preconditioning due to Sea Ice Melt

It has been suggested that, in addition to wind forcing, sea ice and the associated seasonal freshwater input during summer melting have an impact on thermocline dynamics by counterbalancing the wind-driven Ekman downwelling (Daae et al., 2017; Hattermann, 2018; Stewart & Thompson, 2016; Zhou et al., 2014).

A middepth fresh anomaly is observed at all moorings during the second half of 2017 (Figures 2g–2i), resulting in modifications of the vertical density structure on the shelf. This winter freshening is in contrast to the steadily increasing salinity at freezing point temperatures in the previous years (Figures 2g–2i), which had been attributed to a deepening of the mixed layer associated with brine rejection from winter sea ice production (Ryan et al., 2017). Estimates of 2017 (April–September) polynya ice production off Brunt Ice Shelf were not significantly below the multiyear average (Figure 4e). Reduced local sea ice formation and associated reduced salt input during winter are thus likely not the source of the observed fresh anomaly. We hypothesize that this anomaly has been advected into the region from further upstream via the coastal current. This is supported by the difference in the MWDW mixing line suggesting mixing with ESW instead of WW.

Exceptionally low sea ice conditions were observed in summer 2016/2017 in Box_{ups} and Box_{loc} (Figure 4d). Maps of sea ice concentration (Figure S4) show early melting at the Greenwich Meridian in November and continuous melting along the coast with almost no sea ice cover in the southeastern Weddell Sea in

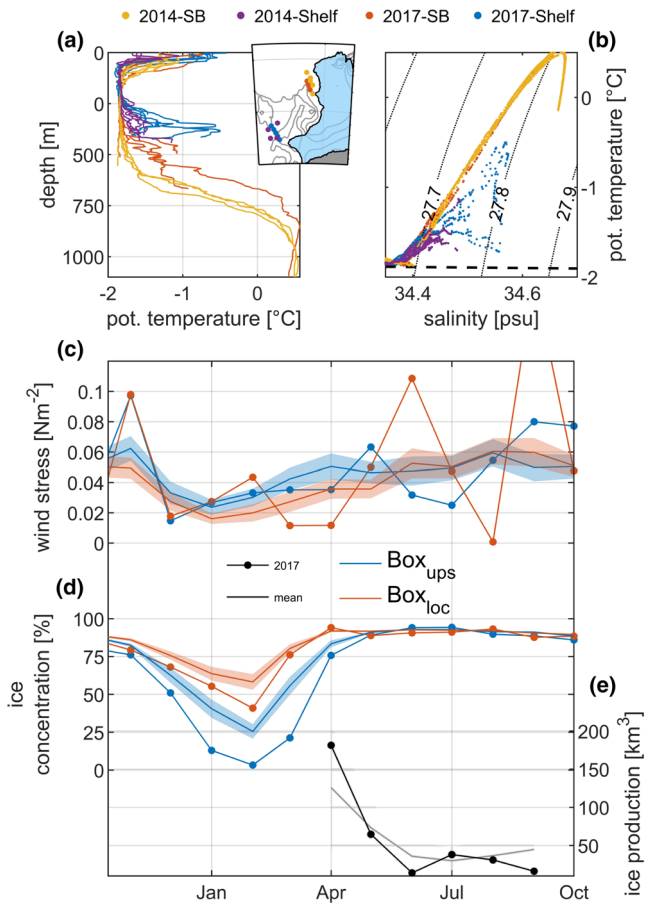

Figure 4. Potential temperature profiles (a) and TS properties (b) of selected stations from 2014 and 2017 in the southeastern Weddell Sea (see inset). Monthly mean along-coast wind stress (c) and mean sea ice concentration (d) in Box$_{ups}$ and Box$_{loc}$ for 2016/2017 compared to long-term mean (solid line). Ice production rates for the eastern shelf for 2017 (e) compared to the long-term mean (2002–2017, solid line). Shading in (c)–(e) denotes the standard error. SB = shelf break.

February. The large-scale melting is likely to induce a freshwater anomaly along the coast due to Ekman transport of the fresh surface layer toward the coast. This is consistent with findings by Graham et al. (2013), who suggest that during summer a fresh anomaly develops near the Fimbul Ice Shelf (0–5°W) which then propagates southwestward along the coast. Assuming a coastal current velocity of 0.1–0.3 m s^{-1} (Graham et al., 2013) and 0.03 m s^{-1} for the Filchner inflow (Darelius et al., 2016; Ryan et al., 2017) the advective time scale from Greenwich Meridian to the mooring location at 76°S ranges from 4–7 months. This is consistent with our observations which show the onset of the fresh anomaly in June/July and maximum in October. Furthermore, large-scale melting occurred along the whole coast upstream, likely causing a freshening of the entire continental shelf along the coast of Dronning Maud Land. Increased baroclinic instabilities along the ASF, due to larger horizontal density gradients, can drive a shoaling of the thermocline (Hattermann, 2018; Nøst et al., 2011) upstream of the FT, consistent with our shelf break observations.

6. Conclusions

Two years of additional mooring observations from the southern Weddell Sea continental shelf (76°S) show an unprecedented long-lasting and warm inflow of MWDW along the eastern flank of the FT in 2017, reaching at least as far south as 77°S. At all moorings, maximum temperatures exceeded −1.0°C, and temperatures around −1.5°C persisted on the continental shelf throughout winter. In contrast, previous observations

showed a return to near-freezing conditions during winter/spring. Shelf break CTD profiles from February 2017 indicate a shoaled thermocline, which likely lead to the onshore transport of deeper and thus warmer MWDW. Darelius et al. (2016) attribute a strong warm inflow in 2013 to persistent below-average alongcoast wind stress that relaxed the shelf break thermocline. These conditions were not observed in 2017. Instead, we propose that freshened shelf waters from upstream along the coast of Dronning Maud Land contributed to the observed shoaling of the thermocline, via increased baroclinic instabilities.

TS properties of the MWDW suggest mixing of WDW with fresher ESW, typically found upstream on the narrow eastern Weddell Sea (Graham et al., 2013), in 2017 instead of WW. In addition, salinities observed in the FT associated with the prolonged inflow, were significantly below the 2014–2016 average. We hypothesize that the low salinity anomaly is an advected rather than a locally forced signal, as estimates of sea ice production in the FT area in the previous winter only showed average values. The anomaly possibly originated from enhanced summer sea ice melting upstream along the coast of Dronning Maud Land, from where it was transported southward within the ASC and ultimately contributed to a shoaling of the thermocline (Daae et al., 2017; Hattermann, 2018; Stewart & Thompson, 2016; Zhou et al., 2014). However, due to the lack of observations upstream, this remains speculative.

Our results suggest that the modified density structure on the continental shelf with lighter densities in the upper 400 m favors an earlier onset of onshore flow of MWDW at greater depth in 2018. This mechanism is different from the processes proposed by Hellmer et al. (2017), who suggested that less sea ice formation on the southern Weddell Sea continental shelf and associated decrease in ISW density, cause an irreversible flow of MWDW into the FT toward the end of this century. Our study shows that the projected upper ocean freshening, either by enhanced melting of sea ice or fringing ice shelves, along the coast of the eastern Weddell Sea might be an additional if not an earlier threat to the stability of FRIS and highlights a sensitivity to upstream processes, which are more susceptible to the changing climate. Therefore, in addition to continuing the hydrographic monitoring in the FT, upstream observations are urgently needed to constrain our proposed hypothesis and provide a better estimate on the vulnerability of the Antarctic Ice Sheet.

Data Availability Statement

The time series of sea ice production rates up to 2015 is available under https://doi.pangaea.de/10.1594/PANGAEA.848612(Paul et al., 2015a), and the extension will be provided upon request by Dr. Stephan Paul at the Ludwigs-Maximilian University Munich (stephan.paul@lmu.de). ERA-Interim data are available online (from https://apps.ecmwf.int/datasets/data/interim-full-daily/levtype=sfc/). Sea ice data can be downloaded online (at ftp://ftp-icdc.cen.uni-hamburg.de/asi_ssmi_iceconc/ant/). All data supplied by the Alfred Wegener Institute and the Geophysical Institute can be accessed through the PANGAEA database as follows: PS82 (https://doi.org/10.1594/PANGAEA.833319), PS96 (https://doi.org/10.1594/PANGAEA.859040), PS111 (https://doi.org/10.1594/PANGAEA.897280), ES060 (https://doi.org/10.1594/PANGAEA.845032), WAPITI (https://doi.org/10.17882/54012), LoTUS buoy (https://doi.org/10.1594/PANGAEA.890139), and moorings $M_{30.5W}$, M_{31W}, $M_{31.5W}$ (https://doi.org/10.1594/PANGAEA.903104, https://doi.org/10.1594/PANGAEA.903315, https://doi.pangaea.de/10.1594/PANGAEA.903317).

Acknowledgments

The authors would like to express their gratitude to the officers and crews of RV *Polarstern* (cruises PS92 [Grant AWI_PS82_02], PS96 [Grant AWI_PS96_01], and PS111 [Grant AWI_PS111_01]), RRS *Ernest Shackleton* (Cruise ES060), and RSS *James Clark Ross* (Cruise JR16004) for their efficient assistance. Special thanks to Andreas Wisotzki and Gerd Rohardt for the outstanding care with the data sampling and processing. Furthermore, thank you to two anonymous reviewers for their constructive comments that improved the manuscript. E. D. received funding from the project TOBACO (267660), POLARPROG, Norges Forskningsrd. The authors thank the University of Trier, Germany, and Stephan Paul for providing capacities to process the additional daily sea ice production rates for the years 2015 to 2017 following the approach by Paul et al. (2015b).

References

Andreas, E. L., Horst, T. W., Grachev, A. A., Persson, P. O. G., Fairall, C. W., Guest, P. S., & Jordan, R. E. (2010). Parametrizing turbulent exchange over summer sea ice and the marginal ice zone. *Quarterly Journal of the Royal Meteorological Society*, *136*(649), 927–943. https://doi.org/10.1002/qj.618

Årthun, M., Nicholls, K. W., Makinson, K., Fedak, M. A., & Boehme, L. (2012). Seasonal inflow of warm water onto the southern Weddell Sea continental shelf, Antarctica. *Geophysical Research Letters*, *39*, L17601. https://doi.org/10.1029/2012GL052856

Carmack, E. C. (1974). A quantitative characterization of water masses in the Weddell Sea during summer. *Deep-Sea Research and Oceanographic Abstracts*, *21*(6), 431–443. https://doi.org/10.1016/0011-7471(74)90092-8

Daae, K., Hattermann, T., Darelius, E., & Fer, I. (2017). On the effect of topography and wind on warm water inflow—An idealized study of the southern Weddell Sea continental shelf system. *Journal of Geophysical Research: Oceans*, *122*, 2622–2641. https://doi.org/10.1002/2016JC012541

Darelius, E., & Fer, I. (2015). Physical oceanography from CTD in the Filchner depression (Weddell Sea, Antarctica) during Ernest Shackleton Cruise ES060. https://doi.org/10.1594/PANGAEA.846962

Darelius, E., Fer, I., & Nicholls, K. W. (2016). Observed vulnerability of Filchner-Ronne Ice Shelf to wind-driven inflow of Warm Deep Water. *Nature Communications*, *7*, 12,300. https://doi.org/10.1038/ncomms12300

Darelius, E., & Kuttenkueler, J. (2018). Bottom temperature from the southern Weddell Sea measured using an autonomous LoTUS buoy. PANGAEA. https://doi.org/10.1594/PANGAEA.890139

Darelius, E., Makinson, K., Daae, K., Fer, I., Holland, P. R., & Nicholls, K. W. (2014). Hydrography and circulation in the Filchner depression, Weddell Sea, Antarctica. *Journal of Geophysical Research: Oceans*, *119*, 5797–5814. https://doi.org/10.1002/2014JC010225

Darelius, E., & Sallée, J. B. (2018). Seasonal outflow of ice shelf water across the front of the Filchner Ice Shelf, Weddell Sea, Antarctica. *Geophysical Research Letters*, *45*, 3577–3585. https://doi.org/10.1002/2017GL076320

Dee, D. P., Uppala, S. M., Simmons, A. J., Berrisford, P., Poli, P., Kobayashi, S., et al. (2011). The ERA-Interim reanalysis: Configuration and performance of the data assimilation system. *Quarterly Journal of the Royal Meteorological Society*, *137*(656), 553–597. https://doi.org/10.1002/qj.828

Fürst, J. J., Durand, G., Gillet-Chaulet, F., Tavard, L., Rankl, M., Braun, M., & Gagliardini, O. (2016). The safety band of Antarctic ice shelves. *Nature Climate Change*, *6*(5), 479–482. https://doi.org/10.1038/nclimate2912

Fahrbach, E., Peterson, R. G., Rohardt, G., Schlosser, P., & Bayer, R. (1994). Suppression of bottom water formation in the southeastern Weddell Sea. *Deep Sea Research Part I: Oceanographic Research Papers*, *41*(2), 389–411. https://doi.org/10.1016/0967-0637(94)90010-8

Foldvik, A. (2004). Ice shelf water overflow and bottom water formation in the southern Weddell Sea. *Journal of Geophysical Research*, *109*(2), C02015. https://doi.org/10.1029/2003JC002008

Foldvik, A., & Gammelsrød, T. (1988). Notes on Southern Ocean hydrography, sea-ice and bottom water formation. *Palaeogeography, Palaeoclimatology, Palaeoecology*, *67*(1), 3–17. https://doi.org/10.1016/0031-0182(88)90119-8

Gill, A. E. (1973). Circulation and bottom water production in the Weddell Sea. *Deep-Sea Research and Oceanographic Abstracts*, *20*(2), 111–140. https://doi.org/10.1016/0011-7471(73)90048-X

Graham, J. A., Heywood, K. J., Chavanne, C. P., & Holland, P. R. (2013). Seasonal variability of water masses and transport on the Antarctic continental shelf and slope in the southeastern Weddell Sea. *Journal of Geophysical Research: Oceans*, *118*, 2201–2214. https://doi.org/10.1002/jgrc.20174

Hattermann, T. (2018). Antarctic thermocline dynamics along a narrow shelf with easterly winds. *Journal of Physical Oceanography*, *48*(10), 2419–2443. https://doi.org/10.1175/jpo-d-18-0064.1

Hellmer, H. H., Kauker, F., Timmermann, R., Determann, J., & Rae, J. (2012). Twenty-first-century warming of a large Antarctic ice-shelf cavity by a redirected coastal current. *Nature*, *485*, 5–8. https://doi.org/10.1038/nature11064

Hellmer, H. H., Kauker, F., Timmermann, R., & Hattermann, T. (2017). The fate of the southern Weddell Sea continental shelf in a warming climate. *Journal of Climate*, *30*(12), 4337–4350. https://doi.org/10.1175/JCLI-D-16-0420.1

Jacobs, S. S. (1991). On the nature and significance of the Antarctic slope front. *Marine Chemistry*, *35*(1-4), 9–24. https://doi.org/10.1016/S0304-4203(09)90005-6

Janout, M., Hellmer, H. H., Schröder, M., & Wisotzki, A. (2019). *Physical oceanography during POLARSTERN cruise PS111 (ANT-XXXIII/2)*, Bremerhaven, Pangaea: Alfred Wegener Institute, Helmholtz Centre for Polar and Marine Research. https://doi.org/10.1594/PANGAEA.897280

Núñez-Riboni, I., & Fahrbach, E. (2009). Seasonal variability of the Antarctic coastal current and its driving mechanisms in the Weddell Sea. *Deep-Sea Research Part I: Oceanographic Research Papers*, *56*(11), 1927–1941. https://doi.org/10.1016/j.dsr.2009.06.005

Nakayama, Y., Schröder, M., & Hellmer, H. H. (2013). From circumpolar deep water to the glacial meltwater plume on the eastern Amundsen shelf. *Deep-Sea Research Part I: Oceanographic Research Papers*, *77*, 50–62. https://doi.org/10.1016/j.dsr.2013.04.001

Nicholls, K. W., Østerhus, S., Makinson, K., Gammelsrød, T., & Fahrbach, E. (2009). Ice-ocean processes over the continental shelf of the southern Weddell Sea, Antarctica: A review. *Reviews of Geophysics*, *47*(3), 1–23. https://doi.org/10.1029/2007RG000250

Nøst, O. A., Biuw, M., Tverberg, V., Lydersen, C., Hattermann, T., Zhou, Q., et al. (2011). Eddy overturning of the Antarctic slope front controls glacial melting in the eastern Weddell Sea. *Journal of Geophysical Research*, *116*(11), C11014. https://doi.org/10.1029/2011JC006965

Paolo, F. S., Fricker, H. A., & Padman, L. (2015). Volume loss from Antarctic ice shelves is accelerating. *Science*, *348*(6232), 327–332. https://doi.org/10.1126/science.aaa0940

Paul, S., Willems, S., & Heinemann, G. (2015a). Daily MODIS composites of thin-ice and ice-surface temperatures for the southern Weddell Sea. PANGAEA, https://doi.org/10.1594/PANGAEA.848612

Paul, S., Willmes, S., & Heinemann, G. (2015b). Long-term coastal-polynya dynamics in the southern Weddell Sea from MODIS thermal-infrared imagery. *The Cryosphere*, *9*(6), 2027–2041. https://doi.org/10.5194/tc-9-2027-2015

Pritchard, H. D., Ligtenberg, S. R. M., Fricker, H. A., Vaughan, D. G., Broeke, M. R. V. D., & Padman, L. (2012). Antarctic ice-sheet loss driven by basal melting of ice shelves. *Nature*, *484*(7395), 502–505. https://doi.org/10.1038/nature10968

Reid, J. L., & Lynn, R. J. (1971). On the influence of the Norwegian-Greenland and Weddell Seas upon the bottom waters of the Indian and Pacific Oceans. *Deep Sea Research and Oceanographic Abstracts*, *18*(11), 1063–1088. https://doi.org/10.1016/0011-7471(71)90094-5

Rignot, E., Jacobs, S., Mouginot, J., & Scheuchl, B. (2013). Ice-shelf melting around Antarctica. *Science*, *341*(6143), 266–270. https://doi.org/10.1126/science.1235798

Rignot, E., Mouginot, J., Scheuchl, B., Van Den Broeke, M., Van Wessem, M. J., & Morlighem, M. (2019). Four decades of Antarctic ice sheet mass balance from 1979–2017. *Proceedings of the National Academy of Science*, *116*(4), 1095–1103. https://doi.org/10.1073/pnas.1812883116

Ryan, S., Hattermann, T., Darelius, E., & Schröder, M. (2017). Seasonal cycle of hydrography on the eastern shelf of the Filchner trough, Weddell Sea, Antarctica. *Journal of Geophysical Research: Oceans*, *122*, 6437–6453. https://doi.org/10.1002/2017JC012916

Sallée, J. B. (2018). *Hydrological and current data for the southern Weddell Sea, collected as part of the WAPITI oceanographic survey (jr16004)*, Paris: SEANOE. https://doi.org/10.17882/54012

Schröder, M., Ryan, S., & Wisotzki, A. (2016). Physical oceanography during POLARSTERN cruise PS96 (ANT-XXXI/2 FROSN). https://doi.org/10.1594/PANGAEA.859040

Schröder, M., & Wisotzki, A. (2014). Physical oceanography during POLARSTERN cruise PS82 (ANT-XXIX/9). https://doi.org/10.1594/PANGAEA.833299

Sloyan, B. M., & Rintoul, S. R. (2001). The Southern Ocean limb of the global deep overturning circulation*. *Journal of Physical Oceanography*, *31*(1), 143–173. https://doi.org/10.1175/1520-0485(2001)031%3C0143:TSOLOT%3E2.0.CO;2

St-Laurent, P., Klinck, J. M., & Dinniman, M. S. (2013). On the role of coastal troughs in the circulation of warm circumpolar deep water on Antarctic shelves. *Journal of Physical Oceanography*, *43*(1), 51–64. https://doi.org/10.1175/JPO-D-11-0237.1

Stewart, A. L., Klocker, A., & Menemenlis, D. (2018). Circum-Antarctic shoreward heat transport derived from an eddy- and tide-resolving simulation. *Geophysical Research Letters*, *45*, 834–845. https://doi.org/10.1002/2017GL075677

Stewart, A. L., & Thompson, A. F. (2015). Eddy-mediated transport of warm circumpolar deep water across the Antarctic shelf break. *Geophysical Research Letters*, *42*, 432–440. https://doi.org/10.1002/2014GL062281

Stewart, A. L., & Thompson, A. F. (2016). Eddy generation and jet formation via dense water outflows across the Antarctic continental slope. *Journal of Physical Oceanography*, *46*(12), 3729–3750. https://doi.org/10.1175/jpo-d-16-0145.1

Thompson, A. F., Stewart, A. L., Spence, P., & Heywood, K. J. (2018). The Antarctic slope current in a changing climate. *Reviews of Geophysics*, *56*, 741–770. https://doi.org/10.1029/2018RG000624

Timmermann, R., & Hellmer, H. H. (2013). Southern Ocean warming and increased ice shelf basal melting in the twenty-first and twenty-second centuries based on coupled ice-ocean finite-element modelling. *Ocean Dynamics*, *63*(9-10), 1011–1026. https://doi.org/10.1007/s10236-013-0642-0

Zhou, Q., Hattermann, T., Nøst, O. A., Biuw, M., Kovacs, K. M., & Lydersen, C. (2014). Wind-driven spreading of fresh surface water beneath ice shelves in the eastern Weddell Sea. *Journal of Geophysical Research: Oceans*, *119*, 3818–3833. https://doi.org/10.1002/2013JC009556